tvst

Article

Longitudinal Assessment of Alkali Injury on Mouse Cornea Using Anterior Segment Optical Coherence Tomography

Jonathan Luisi[1], Edward R. Kraft[1], Steven A. Giannos[1], Krishna Patel[2], Mary E. Schmitz-Brown[1], Valentina Reffatto[1], Kevin H. Merkley[1], and Praveena K. Gupta[1]

[1] Department of Ophthalmology and Visual Sciences, University of Texas Medical Branch, Galveston, TX, USA
[2] School of Medicine, University of Texas Medical Branch, Galveston, TX, USA

Correspondence: Praveena K. Gupta, Department of Ophthalmology and Visual Sciences, University of Texas Medical Branch, 301 University Boulevard, Galveston, TX 77555, USA. e-mail: prgupta@utmb.edu

Received: October 13, 2020
Accepted: January 24, 2021
Published: March 9, 2021

Keywords: alkali burn; sodium hydroxide; ocular injury; optical coherence tomography; fluorescein angiography; Descemet's membrane detachment; anterior-segment OCT; OCT angiography; cornea opacity; corneal neovascularization; epithelial bullae

Citation: Luisi J, Kraft ER, Giannos SA, Patel K, Schmitz-Brown ME, Reffatto V, Merkley KH, Gupta PK. Longitudinal assessment of alkali injury on mouse cornea using anterior segment optical coherence tomography. Trans Vis Sci Tech. 2021;10(3):6, https://doi.org/10.1167/tvst.10.3.6

Purpose: Chemical burns due to alkalis cause extensive damage to the ocular surface leading to blindness. Assessment of ocular burn could be challenging due to severe opacity, inflammation, and angiogenesis. Anterior segment optical coherence tomography (AS-OCT) and OCT angiography (OCTA) may provide fast, non-invasive deep tissue visualization of pathology with high sensitivity in conjunction with slit-lamp analysis.

Methods: C57-BL/6J mice were anesthetized with ketamine/dexmedetomidine, and corneal alkali burn was induced ($n = 6$) by placing filter paper soaked in 1-M sodium hydroxide for 30 seconds on the right eye while the left eye was kept as control. Longitudinal imaging was done with AS-OCT/OCTA and fluorescein angiography at various time intervals for 14 days.

Results: AS-OCT showed characteristic pathological changes in alkali-burned eyes with high sensitivity. Although OCT/OCTA showed three-dimensional and cross-sectional views of the anterior chamber and angiogenesis, fluorescein angiography showed nascent vessels with active leakage. Corneal swelling progressively increased by 125.26% on day 12 with a high prevalence of epithelial bullae, stromal cysts, stromal splitting, and Descemet's membrane detachment. Neovascularization was noted as early as day 4 in the burned eyes by both methods. Severe corneal opacity and anterior chamber inflammation were also detected by AS-OCT/OCTA.

Conclusions: AS-OCT/OCTA is a promising, noninvasive, high-resolution imaging modality that can provide both qualitative and quantitative information regarding deep tissue pathology at a structural level.

Translational Relevance: Noninvasive AS-OCT/OCTA and fluorescein methods show promise in clinical pathology evaluation for ocular injury management and prognostic indications, as the early presence of Descemet's membrane detachment and corneal swelling appears to be correlated with the severity and localization of corneal neovascularization.

Introduction

The cornea is the most anterior part of the eye and it must be transparent for good visual acuity. Its unique avascular characteristics and precise arrangement of collagen fibers prevent light from scattering, resulting in a focused image on the retina. A chemical injury to the cornea can threaten the transparency of the cornea via inflammation, neovascularization, and permanent scarring.[1] Exposure to any acidic and alkaline chemicals can inflict a burn to the eye; however, alkalis are known to cause more severe burns than acids. This is due to the lipophilic nature of the alkali agents that helps them penetrate deeper into the tissues.[2,3] Alkali burns can result from accidental exposure to sodium hydroxide (lye, which can be found in drain cleaners and industrial cleaning solutions), ammonia (found in household cleaning solutions and fertilizers), and calcium hydroxide (lime, which can

be found in cement and plaster). Other risk factors that can compromise the health of the cornea include wearing contact lens too long, ocular surface disease, trauma, surgical complications, and infections such as herpes.[4]

Ocular chemical burns trigger a cascade of events, including infiltration of neutrophils, epithelial cell loss, ulceration, and stromal lysis which may eventually lead to inflammation, corneal opacity, and neovascularization.[5] Vascular endothelial growth factor (VEGF) produced in response to inflammation paves the way for new blood vessel formation and angiogenesis. A slit-lamp exam is the standard method traditionally used to assess these processes in a clinical setting; however, slit-lamp analysis has its limitations, including poor depth analysis and obstruction of view in cases of tissue scarring. Anterior segment optical coherence tomography (AS-OCT) has been commercially available since 2014 but has been used primarily to diagnose posterior segment diseases and less frequently for anterior segment analysis. Only a handful of studies have explored the use of AS-OCT to demonstrate corneal neovascularization,[6,7] iris melanoma,[8] and tissue remodeling after pterygium surgery,[9] as well as in the detection of Descemet's membrane detachment (DMD).[10]

In this study, we present the application of AS-OCT to assess the qualitative and quantitative changes in the anterior segment and cornea after an acute alkali burn using a mouse model. Additionally, we also utilized fluorescein angiography (FA), and OCT angiography (OCTA) to assess neovascularization in real time. Moreover, we highlight the difference in data acquisition between the two technologies when it comes to in-depth morphology and angiogenesis evaluation.

Materials and Methods

Animal Studies

All animals were handled in accordance with ARVO Statement for the Use of Animals in Ophthalmic and Vision Research, and our procedures were approved by the Institutional Animal Care and Use Committee of University of Texas Medical Branch, Galveston, TX.

Mouse Model of Alkali Burn

Anesthesia was initiated by ketamine (70 mg/kg of body weight) and dexmedetomidine (0.25 mg/kg) injection intraperitoneally and was subsequently maintained for deep anesthesia using inhaled isoflurane administered by breathing mask. Briefly, alkali burn was induced by applying sodium hydroxide (NaOH)-soaked filter paper (2-mm paper circles soaked in 1.0-M NaOH) for 30 seconds on the right eye of C57BL/6 mice ($n = 6$) as described by Anderson et al.[11] The control eyes (left eyes) were treated with paper circles soaked in phosphate-buffered saline. Following treatment, the eyes were flushed with 20 mL saline solution slowly and then covered with one drop of gentamicin sulfate solution. A pain management plan was implemented with subcutaneous sustained-release buprenorphine immediately after the procedure. The contralateral eyes served as control and received similar treatments, without burn.

Imaging Studies

The progression of corneal injury was assessed by gross ophthalmic exam under a stereo microscope and anterior segment imaging (without any hardware modification), documented at baseline and post-burn injury at days 0, 4, 7, 12, and 14. A 3-mm area was volumetrically scanned, and the regions of interest (ROIs) selected for analysis compensated for variance induced by differences in eye size.

Fluorescein Imaging Analysis

Fluorescein imaging was performed at each interval using a Spectralis HRA+OCT system (Heidelberg Engineering, Heidelberg, Germany) with a 30° lens without modification in the 488-nm fluorescent mode. Fluorescein dye was injected intraperitoneally (10 µL of 1:20 saline dilution from 10% 100 mg/mL), and images were captured at 1, 3, and 5 minutes for early through late phase detection. Of the time points, early-phase FA was most consistent for quantification of vascular area. The corneal ROIs in the FA images were manually identified, then automated for threshold. The threshold image was used to compare percent area versus the intensity (arbitrary units). The measurements were compiled for analysis in Excel (Microsoft Corporation, Redmond, WA).

OCTA Imaging Analysis

The cornea and iris were simultaneously imaged using spectral-domain OCT (Envisu R2200; Bioptigen, Durham, NC) with an 18-mm telecentric lens. Two profiles were used: a widefield scan and a repeated three

B-scan mode. The resolution was isotropic respective to the en face view. The repeated scan was processed for OCTA data, with a customized standard deviation and mean average for en face segmentation. Post-image acquisition, analysis of all OCT images was done in ImageJ (National Institutes of Health, Bethesda, MD) using automated scripts for repeatability, and all of the images were registered to reduce motion artifacts before B-scan measurements or OCTA processing. Corneal swelling was quantified by measuring the overall thickness of the cornea from an average of 10 B-scans crossing the central axis of the cornea. Nine locations drawn perpendicular to the surface of the cornea were measured and averaged to account for regional variations. The data were then divided into day 0 (the day of the burn prior to the injury), day 4, day 7, day 12, and day 14. Excel was used to plot the change in corneal thickness over time.

Assessment of Relative Flow Within Vessels in OCTA

The OCT volume scans were processed using a custom OCTA algorithm with the ability to detect vasculature, flowing fluids, and corneal opacity.[12] The 3-frame volume data were averaged by two different frame projection methods to compute the relative flow (standard deviation projection) and static structures (median averaged projection images) in the OCTA. OCTA vasculature was processed for three-dimensional (3D) identification of the neovascularization. The standard deviation averaging method was used to project the volume from 300 slices to a two-dimensional image. The projection images demonstrated vessel density quantification in a way that could be compared to the FA image quantification. Following FA, the percentage of area occupied by the vessels divided by the ROI was calculated for all images. The ROI of the cornea was manually identified, a binary mask was created, and the intensity profile was calculated. The binary mask percent area corresponded to the vessel area within the total corneal area.

Assessment of Corneal Opacity in OCTA

The frame-averaged OCTA method is sensitive to opacity changes. The ROI for vessel area created for the vessel area calculation was used to quantify corneal opacity area. The OCT intensity is related to opacity and corneal occlusions. Within the ROI, the areas of the binary mask and OCT contrast were automatically measured with ImageJ. The ratios of opacity to binary area were calculated to separate cloudy corneas from clear ones.

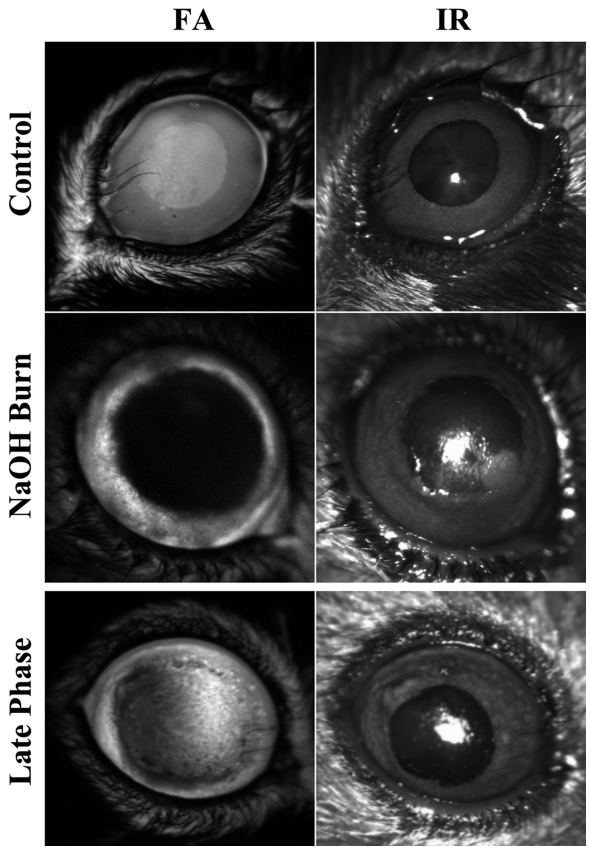

Figure 1. FA and simultaneous IR show the immediate pathology in the cornea following burn. In the control eye at the FA late phase, the pupil is visible and diffusion is uniform. The IR image shows a clear round pupil, and the iris has a uniform texture. Early-phase FA of NaOH burns shows a ring from the limbus and attenuation in the central cornea; IR shows the ring of the burn and defects of the epithelium. Late-phase FA shows the limbus ring and hazy staining corresponding to the burn ring.

Histology

At day 14, eyes were enucleated and fixed in 4% paraformaldehyde. Eyes were embedded in paraffin, sectioned at 7 µm, and stained with hematoxylin and eosin. Sections were imaged with an Olympus IX71 (Olympus Corporation, Tokyo, Japan) in a brightfield configuration of 20× (0.8-µm resolution).

Statistics

Corneal thickness measurements were normalized as percent change per subject and then plotted as box plots. Analysis of variance (ANOVA) and paired Student's *t*-tests showed that the changes were significant at all points.

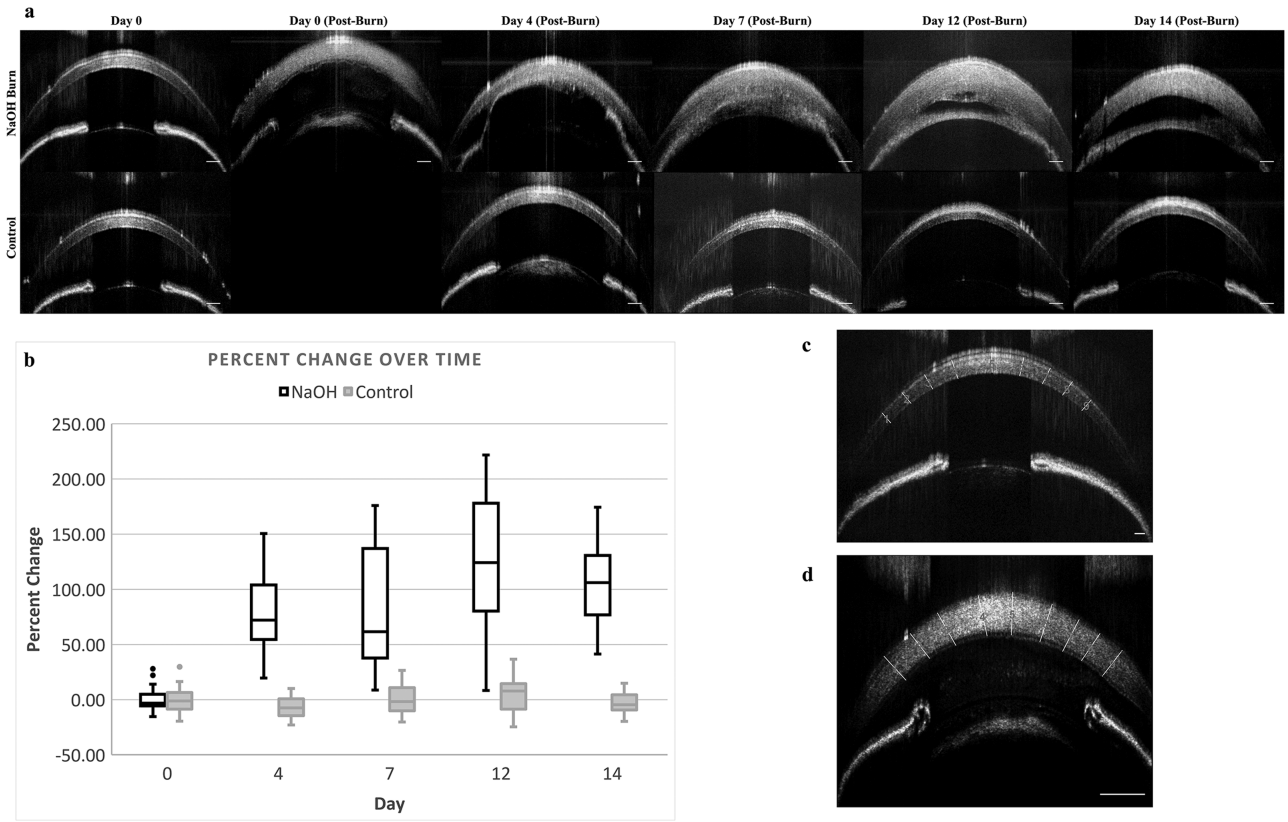

Figure 2. (a) Representative images of averaged B-scans from AS-OCT of a control and post-burn mouse at 0-, 4-, 7-, 10-, and 14-day time intervals. Note the evidence of progressive swelling of the cornea with distinct morphological changes. (b) Box plot of the average thickness of the cornea as percent change with time (thickness presented as an average of nine areas, measured from anterior to posterior reflectivity), control (c) and 1 day (post-burn). $P < 0.005$ for days 4 to 14.

Results

Macroscopic Assessment of the Anterior Segment of the Eye

Alkali burn using 1-M NaOH caused severe burn injury to both the cornea and other deeper structures of the anterior segment. On gross examination, extensive loss of epithelial tissue was instantaneously evident in all of the eyes burned. The control eyes, without burn, showed only focal dry eyes spots with insignificant epithelial loss. Corneal opacity is a confounding factor due to anesthesia and subsequent dry eye and lowers the signal-to-noise ratio; however, comparison of the control and burned eyes was improved upon further analysis (see Methods section). In subsequent days, the corneas of the burned eyes became cloudy with noticeable prominent limbal vessel engorgement. By day 7, all of the injured cornea became opaque to transilluminating light, and visibility of the pupil was also obscured. Both OCTA and AS-OCT detailed morphological changes of the burned cornea. AS-OCT/OCTA provided high-definition, cross-sectional images of the opacity and vasculature in the anterior segment of the eye at all time points, whereas the FA/OCT combination provided information on leaking blood vessels at various time phases (Fig. 1). FA/infrared (IR) imaging provides an intermediate step in the corneal burn model, as OCTA is not widely available in the clinical setting.

Corneal Thickness

Cross-sectional images obtained by B-scan OCT allowed for thickness measurement of the cornea, as mentioned earlier in Methods. The thickness of the cornea continued to increase immediately post-burn and peaked at day 12 (125.26% ± 57% change) and showed regression at day 14 (103.49% ± 34% change) (see representative image in Fig. 2a). The average mean swelling of each cornea was plotted over time in a box plot (Fig. 2b).

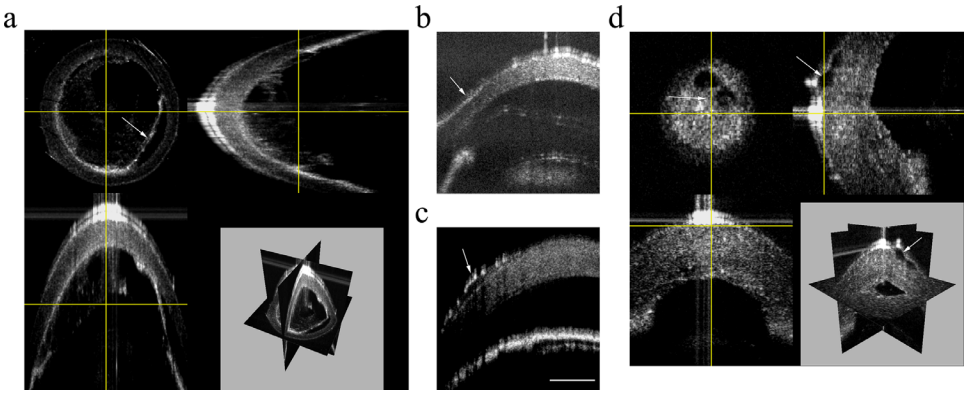

Figure 3. En face, cross-sectional, and orthogonal views using OCTA imaging in a representative mouse assessed at day 7. (a) Arrows point to the DMD and hyper- and hyporeflective areas, which indicate a loss of structural homogeneity. (b, c) Arrows point to epithelial surface irregularity. (d) Hyporeflective area shows the presence of epithelial bullae in different views.

Epithelial Defects

Although the Spectralis FA and IR en face images show gross structural changes of the cornea, including atrophied geographic area and corneal opacity, OCTA imaging was able to assess depth-resolved 3D morphology of the cornea to delineate various layers at day 7 (Fig. 3a). Of note, severe epithelial desurfacing was noted as irregular areas early on after alkali burn (Figs. 3b, 3c). The presence of local epithelial bullae was noted by day 4 (Fig. 3d). The control eyes also showed some desurfacing of epithelial cells due to dry eye and anesthesia.

Stromal Disintegration

Loss of homogeneity of stromal fibers was visible in all burned eyes when compared to non-burned eyes in the B-scan images captured by OCTA. Uneven hyperreflectivity and hyporeflectivity within the stromal architecture was noted between day 4 and day 7 post-burn in all NaOH-burned eyes, representing primarily fluid-filled pockets in the stroma. By day 12, all of the burned eyes showed bullous keratopathy, with full separation of stroma from the Descemet's membrane (Figs. 4a, 4d).

Descemet's Membrane Detachment

Detachment of Descemet's membrane was another common finding of deep tissue damage after the acute alkali burn in mice. This phenomenon was visualized around day 4 post-burn as a local splitting of the DM, which subsequently progressed to complete detachment by day 12 in 75% of burned eyes (Figs. 4b, 4d).

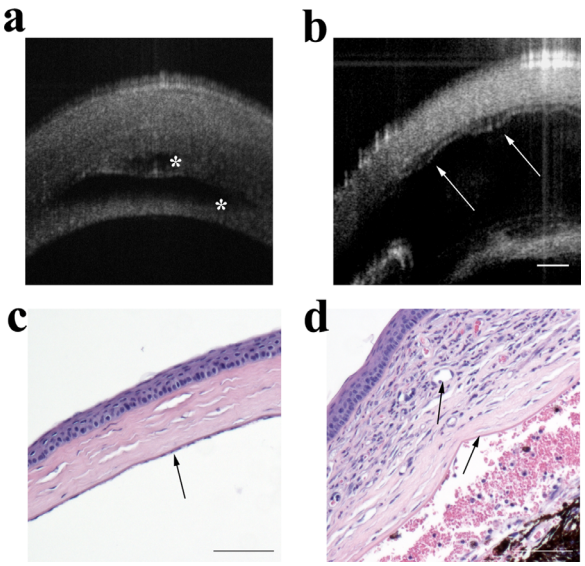

Figure 4. High-resolution, cross-section OCTA image of cornea. (a) Corneal edema and hyporeflective stromal cyst and stromal fluid pocket. (b) At day 7 of a representative mouse (*asterisk*), thin, irregular, hyperreflective DMD 4-days post-burn (*arrow*) is apparent. To verify the pathology, histology slides at day 14 were assessed at 10×. (c) Normal corneal thickness and endothelial cells are readily visible. (d) In contrast, the burned eye has increased stromal thickness, endothelial cell stripping, and DMD; pathology includes neovascularization and infiltration of red blood cells in the cornea. Also note the presence of inflammation with white and red blood cells in the anterior chamber.

Morphological Evaluation of the Anterior Chamber

The corneal burn also induced severe inflammatory reaction in the anterior chamber in 75% of eyes with burn. Evidence of white blood cells in the anterior chamber was noted at day 7 post-burn, indicating

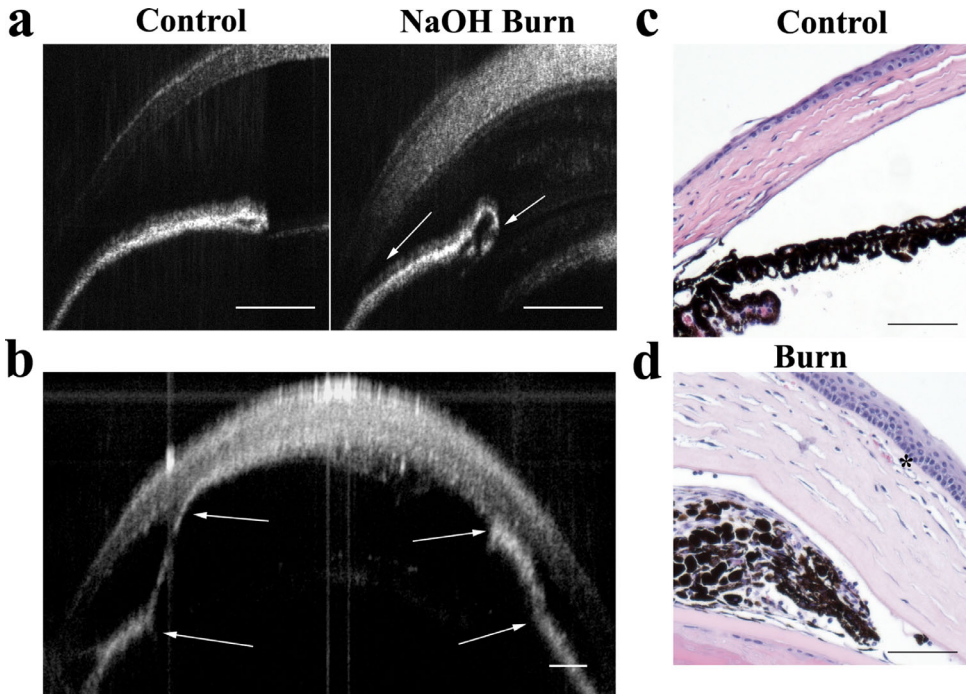

Figure 5. High-resolution, cross-section images of OCTA showing examples from a control and a burned cornea. (a) The burned cornea is appreciably swollen with epithelial bullae, Descemet's membrane splitting, and a narrow angle (*arrow*) at day 4 post-burn. (b) With time, the eye of the same animal progressively worsened to anterior synechiae (*arrows*) and deteriorated to increased corneal swelling (day 7). (c) The control eye at day 14 showed no alterations to the iris root or corneal thickening. (d) Day 14 post-burn shows iris swelling, synechia, narrowing of the angle, epithelial keratinization, and neovascularization (*asterisk*).

the onset of uveitis. Two of the mice had anterior synechiae with possible angle-closure glaucoma (Fig. 5).

Neovascularization

Migration of fine vessels from the limbal area were evident on day 4 post-burn in all of the burned eyes as detected using both FA/OCT and OCTA. These vessels looked engorged at the limbal area and branched into fine tortuous capillaries that often arborized when encroaching toward the center of the cornea. On the other hand, fine hyperemic limbal vessels were also noted in the control eyes treated with phosphate-buffered saline.

Both OCTA and FA visualized the morphological changes of the neovascularization (Fig. 6). Using FA, arborization and branching of new vessels were seen at the early and mid-phases of FA (at 1 and 3 minutes, respectively) at day 4; however, further characterization was obscured due to fluorescein leaking from the nascent vessels in the late phase (after 5 minutes). OCTA showed the vessels infiltrating from the limbus into the corneal space. On further follow-up, neovascularization intensified, with an increase in vessel tortuosity, branching, and widening in vessel diameter leading to active leakage. In addition, the vessels tended to be denser in the limbal margin and invaded the central cornea with time. The OCTA methodology used provided metrics for both vessel area (red) and opacity (green) (Fig. 6a). The vessel percent area and relative vessel signal intensity (measured in arbitrary units) showed a relationship in the scatterplot (Fig. 6b). As shown in Figure 6c, the ratio of percent area to vessel intensity separates control eyes from neovascularization when plotted over time. Because corneal clouding and opacity changes due to anesthesia are confounding factors, the analysis methodology for vessel area was also applied to opacity, first by plotting the OCTA opacity area and intensity (Fig. 6d) and then determining the ratio over time (Fig. 6e). Reusing the ROIs described in the Methods section allowed normalization of the binary masks for vessel area and opacity for ratio analysis at all time points for days 0, 4, 7, 12, and 14 per subject with complete analysis of longitudinal data. These analyses indicated that OCTA data can be quantified in a semi-automatic method to distinguish injured and control eyes, even with confounding factors such as dry eye.

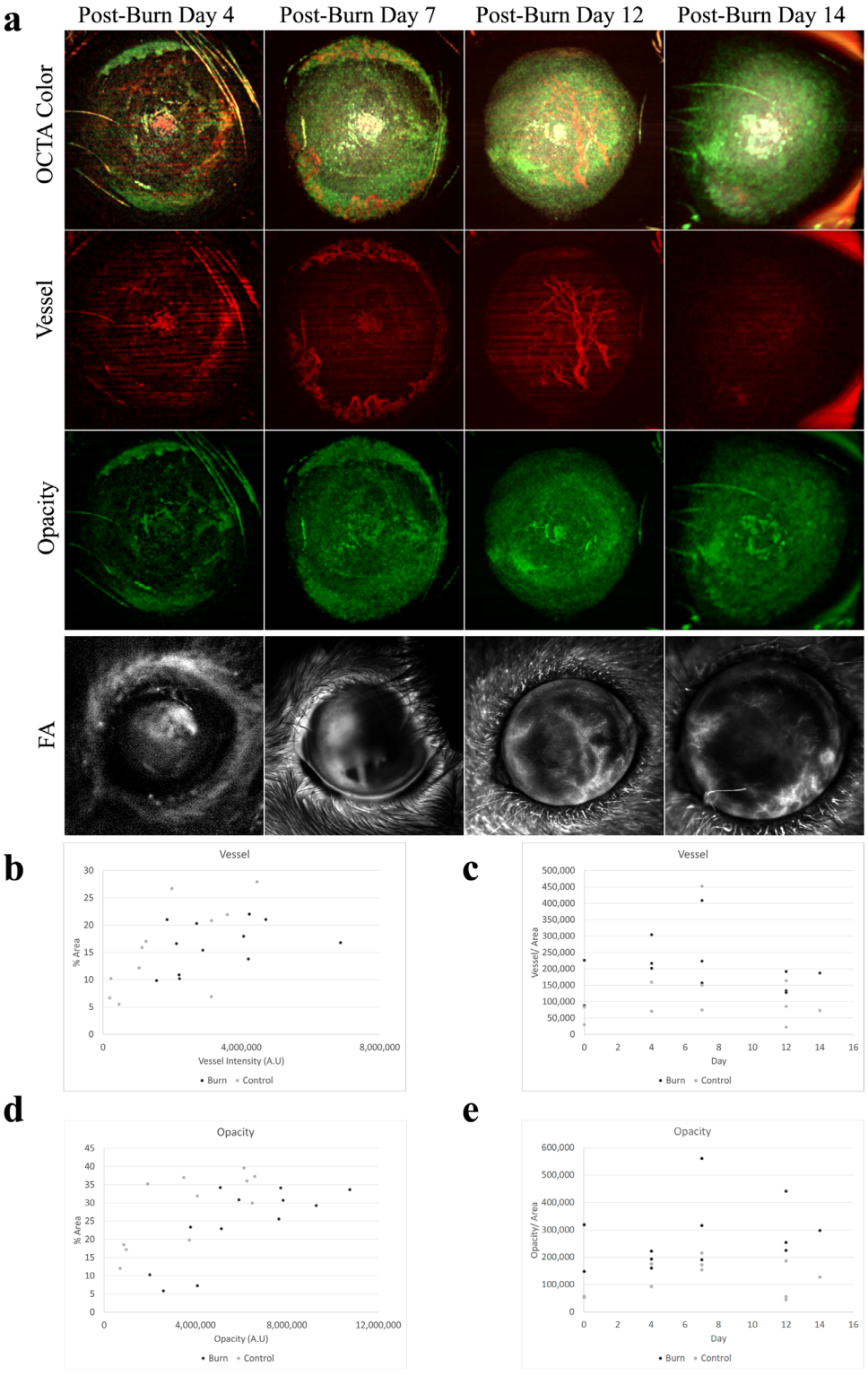

Figure 6. (a) The OCTA and FA data show neovascularization progression over time. Vessels are highlighted by the variable component of the OCTA signal and are shown in *red*. The static component of the OCTA signal is correlated to opacity changes and is shown in *green*. FA revealed the vessels in the early phase and leakage from immature vessels in the late phase. (b) Percent area is plotted against vessel intensity (arbitrary units), demonstrating that the correlation differed between burn and control. (c) The ratio is plotted over time. (d) The opacity (arbitrary units) and percent area are plotted to demonstrate distinguishing between burned eyes and the eyes of controls with dry eye. (e) The ratio is plotted over time to demonstrate the potential for identifying corneal pathologies.

Discussion

This is the first study, to our knowledge, that shows longitudinal real-time pathological details of anterior segment and corneal tissue after an acute alkali burn on a mouse cornea using high-resolution AS-OCT. The information gathered here is critical for our understanding of the cascade of events leading to corneal scarring, and obtaining such information was previously only possible after sacrificing mice at various time intervals. With the aid of AS-OCT imaging, we were able to show superficial punctate epithelial erosions, progressive corneal edema, stromal opacity, DMD, and neovascularization of various extents after the 1-M NaOH alkali burn. In addition, we noted the presence of inflammation in the aqueous humor of the eye, suggesting associated uveitis 7 days after burn injury. In a few isolated cases, we also noted anterior synechiae leading to pupillary block and possible angle-closure glaucoma. With FA/OCT of the anterior segment, we noted extensive perilimbal arborization of vessels and fluorescein leaking at 4 days post-burn.

Although OCT as an imaging tool has been around for 25 years, adapting it to detect anterior segment diseases has not been explored to full extent. Using an acute alkali burn mouse model, we demonstrated the power of this non-invasive imaging tool to assess microscopic pathology of the anterior segment.

Our findings are consistent with those of other studies that have reported similar findings but used a combination of methods, such as slit lamp, color photographs, and sacrificing animals at various time intervals. Bai et al.[13] used various concentrations of NaOH to induce corneal burn. They reported that corneal neovascularization started at day 3 after 1-M NaOH burn, and by day 7 all of the corneas with burn were densely opacified. Conventional protocols commonly use high-concentration alkali (1-M NaOH) to soak filter paper discs, which are then placed on mouse, rat, or rabbit eyes for approximately 30 seconds.[5,11,14] In mice, low-concentration alkali (0.1-M to 0.15-M NaOH) generated grade II burns.[13] However, in other studies, 0.1-M and 0.2-M NaOH induced opacity between days 1 to 3, and neovascularization was measured between day 3 to day 7. Vascular budding was reported on day 2.[15,16] Such discrepancies in observations are expected due to the use of non-standardized methods for assessing ocular burns.

The presence of DMD with subsequent corneal edema can be detected due to the salient clinical features on slit-lamp (in a clear cornea) and AS-OCT imaging. Our findings of DMD after an acute NaOH burn in almost all of the mice may be of interest to many clinicians. Identifying the size, location, and severity of DMD is essential to determining the visual prognosis of a patient. DMD may lead to imbibement of aqueous humor to the stromal and epithelial tissues, causing disarray of stromal fibers and breaks in the hemidesmosomes leading to persistent edema. Such events indicate the risk of developing bullous keratopathy in real-world patients who require immediate management.

A late-stage inflammation consequence of chemical burns is corneal neovascularization, as seen in the current study. The in-growth of new blood vessels is mediated by the upregulation of angiogenic cytokines. The enzyme metalloproteinase degrades the basement membrane of the cornea and extracellular matrix, and proteolytic enzymes allow vascular epithelial cells to enter the stromal layer of the cornea. When ocular inflammation occurs, corneal epithelial and endothelial cells, macrophages, and certain inflammatory cells produce angiogenic growth factors, namely VEGF and fibroblast growth factors. VEGF paves the way for new blood vessel formation by upregulating matrix metalloproteinase production by endothelial cells in the limbal vascular plexus.[17] OCTA B-scans were helpful in assessing corneal edema progression with time, and FA/OCT and OCTA detected angiogenesis. FA/OCT could demonstrate leakage of the dye at the late stage. FA done in the late phase can provide information about leaking vessels, depicted as pooling of a hyperfluorescent geographic area. During this phase, though, details on vessel pattern are lost, but this approach does help to provide information about an active live vessel.

A few studies have shown qualitative visualization of anterior segment vascularization by using OCTA.[18–20] Further, studies by Nanji et al.[7] have described the use of OCTA for quantitative determination of the depth and density of corneal neovascularization in a variety of conditions. Zhao et al.[9] also described the use of OCTA for the imaging of marginal corneal vascular arcades. Here, we showed the power of OCTA analysis to distinguish post-burn pathophysiological entities, which otherwise would be difficult using the current gold-standard methods. Although both FA and OCTA can detect capillary networks, the advantage of FA over OCTA is that it can detect vessel leakage, thus differentiating between ghost and nascent vessels.[21,22]

As OCTA is a relatively new diagnostic tool, its sensitivity and specificity to different pathologies have not been rigorously explored. OCTA does have shortcomings, such as being more prone to artifacts and optical distortions due to changes in refractive indices coming off the ocular surface. On the other hand, the

major advantage of OCTA is that it complements FA and is quickly emerging as a noninvasive imaging alternative to FA.[23]

We found that OCTA presented many advantages over FA/OCT in assessing corneal injury. First, OCTA provided in-depth, cross-sectional information useful for exploring angiogenesis and tissue modeling noninvasively. With OCTA, not only were we able to collect 3D models of cornea with direct visualization of the anterior chamber but we were also able to identify specific layers of the cornea regardless of the amount of corneal scarring. On the other hand, FA/OCT was sensitive enough to depict small vessels and delineated active vessels due to fluorescein leakage. FA of the anterior segment can add further information regarding the extent of neovascularization, but it may not be a feasible tool in clinical settings at follow-up appointments. In such cases, OCTA may serve as an alternative diagnostic tool in conjunction with the slit lamp.

OCTA can also help in staging ocular burn injuries and thus contribute to proper diagnosis and treatment. Ocular burn assessment by the Roper Hall or Dua classification system allows prognostic chemical eye injury grading[2,24]; however, these two systems rely on objective measurements of corneal ischemia and opacity alone.[25–27] With the new insights obtained from the current study, perhaps a dose–response ocular chemical injury model can be designed to augment the existing ocular burn grading system using AS-OCT/OCTA systems.

In summary, we evaluated in vivo longitudinal corneal metrics of swelling, opacification, and neovascularization resulting from alkali burns in mice by utilizing AS-OCT with minimally invasive fluorescein or noninvasive OCTA imaging. We found that the sensitivity of the imaging modalities to assess anterior segments resulted in remarkable reproducibility as far as depicting the cascade of events leading to chronic inflammation and scarring of the cornea. Given the useful information that can be gathered by these two anterior segment imaging tools, we believe this study will encourage providers to use OCTA or FA/OCT as an adjunct to standard diagnostic tools for intervention and management of anterior segment diseases.

Acknowledgments

Supported by Robertson-Poth Distinguished Chair Endowment funds in Ophthalmology and an Environmental Toxicology training grant (NIEHS T32ES007254; JL, under the mentorship of Bill Ameredes, PhD). Additional resources and facilities were provided by Massoud Motamedi, PhD.

Disclosure: **J. Luisi,** None; **E.R. Kraft,** None; **S.A. Giannos,** None; **K. Patel,** None; **M.E. Schmitz-Brown,** None; **V. Reffatto,** None; **K.H. Merkley,** None; **P.K. Gupta,** None

References

1. Baradaran-Rafii A, Eslani M, Haq Z, Shirzadeh E, Huvard MJ, Djalilian AR. Current and upcoming therapies for ocular surface chemical injuries. *Ocul Surf*. 2017;15(1):48–64.
2. Dua HS, King AJ, Joseph A. A new classification of ocular surface burns. *Br J Ophthalmol*. 2001;85(11):1379–1383.
3. Ramponi DR. Chemical burns of the eye. *Adv Emerg Nurs J*. 2017;39(3):193–198.
4. Zuhair S, Walid S. Corneal neovascularization: updates on pathophysiology, investigations & management. *Rom J Ophthalmol*. 2019;63(1):15–22.
5. Choi H, Phillips C, Oh JY, et al. Comprehensive modeling of corneal alkali injury in the rat eye. *Curr Eye Res*. 2017;42(10):1348–1357.
6. Ang M, Cai Y, Tan AC. Swept source optical coherence tomography angiography for contact lens-related corneal vascularization. *J Ophthalmol*. 2016;2016:9685297.
7. Nanji A, Redd T, Chamberlain W, et al. Application of corneal optical coherence tomography angiography for assessment of vessel depth in corneal neovascularization. *Cornea*. 2020;39(5):598–604.
8. Skalet AH, Li Y, Lu CD, et al. Optical coherence tomography angiography characteristics of iris melanocytic tumors. *Ophthalmology*. 2017;124(2):197–204.
9. Zhao Z, Yue Y, Zhang S, et al. Optical coherence tomography angiography for marginal corneal vascular remodelling after pterygium surgery with limbal-conjunctival autograft. *Eye (Lond)*. 2020;34(11):2054–2062.
10. Wylegala E, Nowinska A. Usefulness of anterior segment optical coherence tomography in Descemet membrane detachment. *Eur J Ophthalmol*. 2009;19(5):723–728.
11. Anderson C, Zhou Q, Wang S. An alkali-burn injury model of corneal neovascularization in the mouse. *J Vis Exp*. 2014;86:51159.
12. Liu W, Luisi J, Liu H, Motamedi M, Zhang W. OCT-angiography for non-invasive monitoring

of neuronal and vascular structure in mouse retina: implication for characterization of retinal neurovascular coupling. *EC Ophthalmol*. 2017;5(3):89–98.
13. Bai JQ, Qin HF, Zhao SH. Research on mouse model of grade II corneal alkali burn. *Int J Ophthalmol*. 2016;9(4):487–490.
14. Griffith GL, Wirostko B, Lee HK, et al. Treatment of corneal chemical alkali burns with a crosslinked thiolated hyaluronic acid film. *Burns*. 2018;44(5):1179–1186.
15. Zhou SY, Xie ZL, Xiao O, Yang XR, Heng BC, Sato Y. Inhibition of mouse alkali burn induced-corneal neovascularization by recombinant adenovirus encoding human vasohibin-1. *Mol Vis*. 2010;16:1389–1398.
16. Han KE, Park MH, Kong KH, Choi E, Choi KR, Jun RM. Therapeutic effects of three human-derived materials in a mouse corneal alkali burn model. *Cutan Ocul Toxicol*. 2019;38(4):315–321.
17. Krizova D, Vokrojova M, Liehneova K, Studeny P. Treatment of corneal neovascularization using anti-VEGF bevacizumab. *J Ophthalmol*. 2014;2014:178132.
18. Oie Y, Nishida K. Evaluation of corneal neovascularization using optical coherence tomography angiography in patients with limbal stem cell deficiency. *Cornea*. 2017;36(suppl 1):S72–S75.
19. Lee WD, Devarajan K, Chua J, Schmetterer L, Mehta JS, Ang M. Optical coherence tomography angiography for the anterior segment. *Eye Vis (Lond)*. 2019;6:4.
20. Pichi F, Roberts P, Neri P. The broad spectrum of application of optical coherence tomography angiography to the anterior segment of the eye in inflammatory conditions: a review of the literature. *J Ophthalmic Inflamm Infect*. 2019;9(1):18.
21. Brunner M, Romano V, Steger B, et al. Imaging of corneal neovascularization: optical coherence tomography angiography and fluorescence angiography. *Invest Ophthalmol Vis Sci*. 2018;59(3):1263–1269.
22. Ang M, Sim DA, Keane PA, et al. Optical coherence tomography angiography for anterior segment vasculature imaging. *Ophthalmology*. 2015;122(9):1740–1747.
23. Ang M, Cai Y, MacPhee B, et al. Optical coherence tomography angiography and indocyanine green angiography for corneal vascularisation. *Br J Ophthalmol*. 2016;100(11):1557–1563.
24. Roper-Hall MJ. Thermal and chemical burns. *Trans Ophthalmol Soc U K*. 1965;85:631–653.
25. Gupta N, Kalaivani M, Tandon R. Comparison of prognostic value of Roper Hall and Dua classification systems in acute ocular burns. *Br J Ophthalmol*. 2011;95(2):194–198.
26. Dua HS, Ting DSJ, Al Saadi A, Said DG. Chemical eye injury: pathophysiology, assessment and management. *Eye (Lond)*. 2020;34(11):2001–2019.
27. Sharma N, Kaur M, Agarwal T, Sangwan VS, Vajpayee RB. Treatment of acute ocular chemical burns. *Surv Ophthalmol*. 2018;63(2):214–235.